Available online at www.sciencedirect.com

ScienceDirect

journal homepage: www.keaipublishing.com/jtte

Original Research Paper

# A wavelet transform method for studying the energy distribution characteristics of microseismicities associated rock failure

*Yumei Kang* [a,**], *Hongyuan Liu* [b,*], *Md Maniruzzaman A. Aziz* [c], *Khairul Anuar Kassim* [c]

[a] *College of Resources and Civil Engineering, Northeastern University, Shenyang 110004, China*
[b] *School of Engineering, University of Tasmania, Hobart, TAS 7001, Australia*
[c] *Faculty of Civil Engineering, Universiti Teknologi Malaysia, 81310 Skudai, Johor, Malaysia*

## HIGHLIGHTS

- The waveforms of microseismicity signals released during rock failure are recorded using a microseismicity monitoring system.
- A wavelet transform scheme is developed to study the energy distribution characteristics of the monitored microseismicities.
- It is demonstrated that the microseismicity energies are directly related to the damage mechanism of the granite.

## ARTICLE INFO

*Article history:*
Received 4 April 2017
Received in revised form
28 February 2018
Accepted 2 March 2018
Available online 7 February 2019

*Keywords:*
Microseismicity signal
Rock fracture
Wavelet transform
Band energy
Crack

## ABSTRACT

Microseismicity signals released during rock failure process are firstly recorded using microseismicity monitoring system. A wavelet transform scheme is then developed on the basis of the discrete wavelet transform and implemented into MATLAB to study the energy distribution characteristics of the monitored microseismicity signals. The wavelet transform scheme decomposes the recorded microseismicity signals into various wavelets at seven scales and eight frequency bands. The microseismicity energy at each frequency band is then calculated by integrating the wavelets in each scale. It is found that, for the microseismicity signals recorded during the uniaxial loading of the granite, the microseismicity energies are mainly distributed between the bands 7.8125–15.625 kHz, 15.625–31.250 kHz and 31.25–62.5 kHz and the percentages of the released energies at these frequency bands are 8.24%, 62.72%, 28.08% of the total energies, respectively. The results reveal that the microseismicity energies at these levels are directly related to the damage mechanisms of the granite although further studies are need to identify the failure modes. Then these monitored signals were processed using wavelet transformation to find out the frequency distribution rule and the frequency band energy varying rule of the acoustic emission (AE) signals during the different rock damage and failure stages. The rock failure mechanism was interpreted from the perspective of the relationship between AE signal frequency change and crack propagation. The frequency band energy distribution histograms of the microseismicity signals at different damage stages were computed and drawn

* *Corresponding author*. Tel.: +61 3 6226 2113; fax: +61 3 6226 7247.
** *Corresponding author*. Tel.: +86 24 8368 7704; fax: +86 24 8368 7704.
E-mail addresses: kangyumei@mail.neu.edu.cn (Y. Kang), hong.liu@utas.edu.au (H. Liu).
Peer review under responsibility of Periodical Offices of Chang'an University.
https://doi.org/10.1016/j.jtte.2018.03.007

by the energy calculation method of wavelet transformation implemented into MATLAB. The energy percentage of the low frequency band (d7-a7) and that of the dominated frequency band (d4-d6) and their variation rule were analyzed especially. Accordingly, the critical damage point is that the low frequency energy percentage is above a certain threshold. This index could be used as the failure precursor criterion for rock mass instability monitoring and early warning, since it provided a theoretical guidance for evaluating internal damage of rock. Finally, it is concluded that the proposed wavelet transform method may provide a new mean for the characteristics analysis of the microseismicity signals recorded by the microseismicity monitoring system and may stimulate the application of the microseismicity monitoring technology in the geotechnical and mining engineerings through analyzing the energy of the microseismicity signals to understand the law of microseismicity emitted by rockmass.



## 1. Introduction

When a rock specimen is loaded, the applied mechanical energy is transferred into strain energy stored in the rock. If the applied load is big enough, the rock may fail and the strain energy may be dissipated in the forms of fracture energy, surface energy, kinetic energy, etc. Thus, the deformation and fracture process of the rock under loading is actually the energy transformation process. Correspondingly, more and more researchers have been attracted to study the rock engineering problems from the energy point of view. During the rock failure process, part of the accumulated strain energy may be released as a seismic wave, which is the so-called acoustic emission (AE). There is considerable research reported in literatures on AE released during rock fracture and the corresponding AE signal processing (Baddari et al., 2011; Cai et al., 2007; Lockner, 1993). Researchers applied various methods to retrieve accurate moment tensors based on the joint inversion of a family of AE events for their moment tensors and for the sensor amplifications including coupling effects between sensors and specimens (Baddari et al., 2011). The results show more and more accuracy and efficiency. However most of the studies were conducted by loading granite samples in compression. As the granite samples were compressed to failure, the recorded AE pulses served as indicators of latent rock damage. The damage evolution of the granite is associated with the growth of microcracks from stress concentrators such as voids, inclusions and grain contacts, which results in both inelastic strain and AE. The AE signals are then recorded to provide the information of the size, location and deformation mechanisms of the AE events as well as the properties (e.g., velocity, attenuation and scattering) of the medium through which the AE wave has traveled. Since the AE signal is a kind of unstable random one with both frequency and statistical characterization varying at all time, various kinds of signal analysis methods such as frequency spectrum analysis and wavelet analysis are developed in literatures to analyze the recorded AE signals. The frequency spectrum analysis method may be best suited for analyzing stationary signals. For non-stationary signals such as the AE signal, the wavelet analysis is probably the best analysis method. The wavelet analysis is a kind of time and frequency analysis method with good local analysis features in the both time and frequency domains. Till this moment, many researchers have applied the wavelet analysis method in processing and analyzing AE signals in the field of the AE detection technology, proposed a lot of relevant theories, and obtained some significant results (Chorney et al., 2014; Davis et al., 2013; Ding et al., 2004; Guo et al., 2014; Hryciw et al., 2015; Jeong and Jang, 2000; Kwiatek et al., 2014; Ni and Iwamoto, 2002; Prawin and Rao, 2015; Qi et al., 1997; Zou et al., 2015).

There are two main methods for collecting and processing acoustic emission signals: (1) extracting and simplifying the characteristic parameters of acoustic emission signals, and analyzing and processing the acoustic emission using parametric analysis method; (2) collecting the acoustic emission signal waveform and directly analyzing the waveform using time-frequency analysis. In recent years, classical spectrum analysis based on Fast Fourier Transform (FFT) and modern spectrum analysis method represented by wavelet analysis have been applied in the field of acoustic emission of rock and concrete, and many progresses have been achieved (Antonaci et al., 2012; Karimi et al., 2015).

Signal processing is based on spectral analysis by means of the Discrete Fourier Transform (DFT), which is the primary tool of digital acoustic signal processing. A FFT algorithm was used for computing the DFT with reduced execution time using MATLAB. AE signals were recorded with a sampling frequency of $2.5 \times 10^3$ kHz and the number of points to evaluate the FFT was set to $15 \times 10^3$. The obtained frequency spectrum range is between 0 and 1250 kHz. A simple procedure has been adopted in signal filtering by cutting the frequencies below 80 kHz and above 800 kHz to eliminate spurious signal frequencies. This frequency range corresponds to the maximum sensitivity range of the wide-band AE transducers (Antonaci et al., 2012).

However, there is no mature wavelet transform method till this moment for identifying and analyzing AE signals released

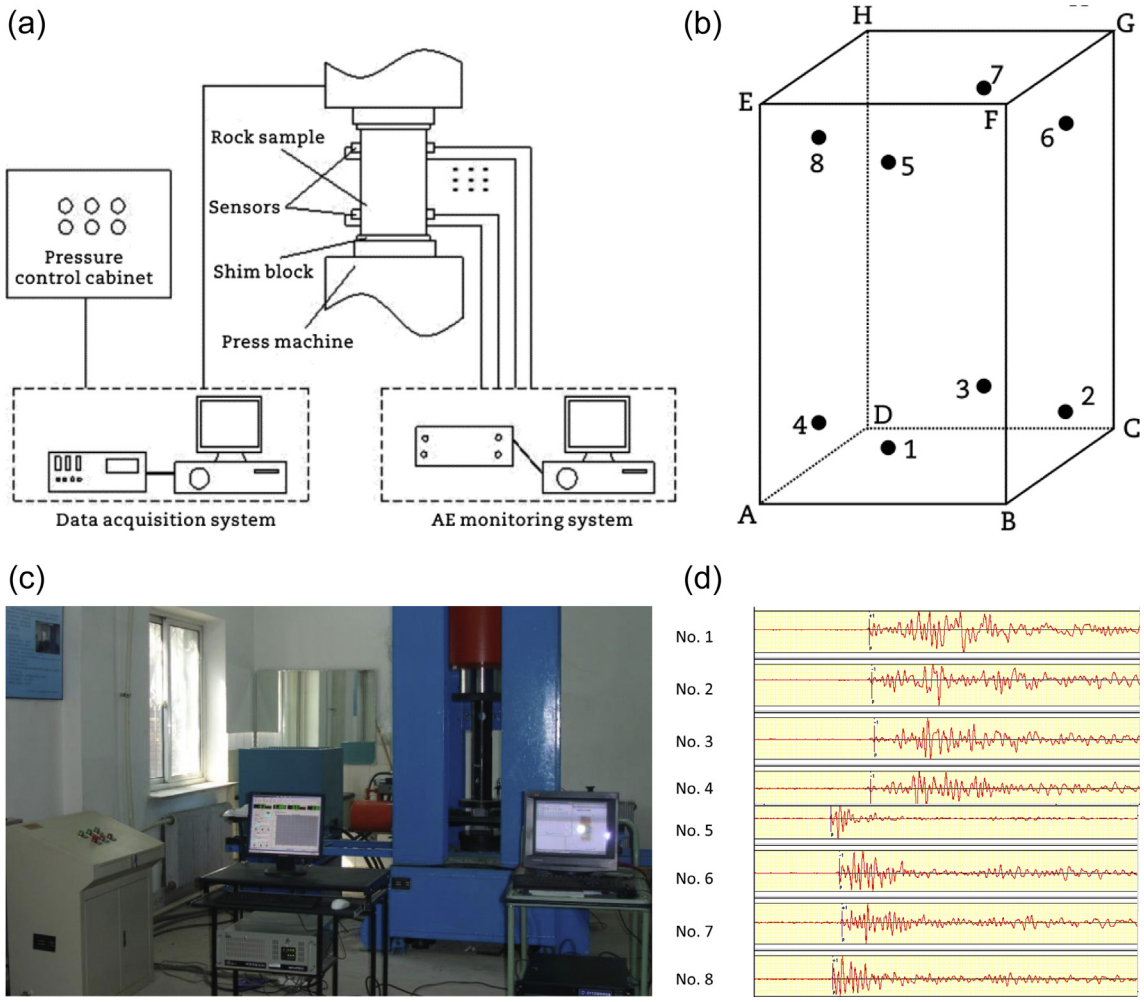


**Fig. 1 – Uniaxial loading of granite and monitored AE signals. (a) Uniaxial loading of granite with AE monitoring. (b) Granite sample with AE sensors (Nos. 1–8). (c) Experimental equipment. (d) A typical AE waveforms collected by 8 sensors. (e) Top view of fractured granite. (f) Top view of AE hypocenters. (g) Front view of fractured granite. (h) Front view of AE hypocenters. (i) Left view of AE hypocenters.**

by rock fracture, especially their energy distribution characteristics, although more and more microseismicity monitoring systems are nowadays installed for daily safety monitoring of various rock engineering applications such as slope stabilities (Amiri et al., 2015; Kalenchuk et al., 2014; Lynch et al., 2005; Rao et al., 2004; Vafaei and Adnan, 2014; Xu et al., 2011), excavation-induced rockbursts (Lesniak and Isakow, 2009; Tang et al., 2011), and oil and gas exploration fields (Basu et al., 2014). The identification and analysis of the rock fracture-induced wavelet directly affect the efficiency and accuracy of the microseismicity monitoring system. In many rock engineering practices, the installed microseismicity monitoring system can't automatically identify valid event log but rely on time-consuming and much less efficient manual processing of onsite engineers. The microseismic waveforms observed in rock engineering are complex and contain multiple confounding factors, which may be easily ignored, mishandled, or not timely analyzed if the manual processing method is relied on. Thus, it becomes more and more important to develop a wavelet transform method to accurately and effectively process the waveforms recorded by the microseismic monitoring system in rock engineering. The AE signals recorded during laboratory rock failure tests are similar to the microseismicity logged by the microseismicity monitoring system in rock engineering applications (Kalenchuk et al., 2014; Rao et al., 2004). Thus, the effective and accurate analysis of the AE signals recorded in laboratory should contribute to the identification of failure events in the waveforms logged by the microseismicity monitoring system.

Although the application of acoustic emission has become more and more popular, and great progresses have been achieved in the development and application acoustic emission monitoring equipment, there are still many problems to be solved in order to apply the acoustic emission to predict and forecast rock engineering instability, especially real-time monitoring and early warning. For example, due to the lack of the reliable criterion of damage precursors and related theoretical basis, the success rate of monitoring and forecasting rock engineering instability is usually low, and the effectiveness of the forecasting is often questioned. Therefore, from the perspective of the application of the acoustic emission

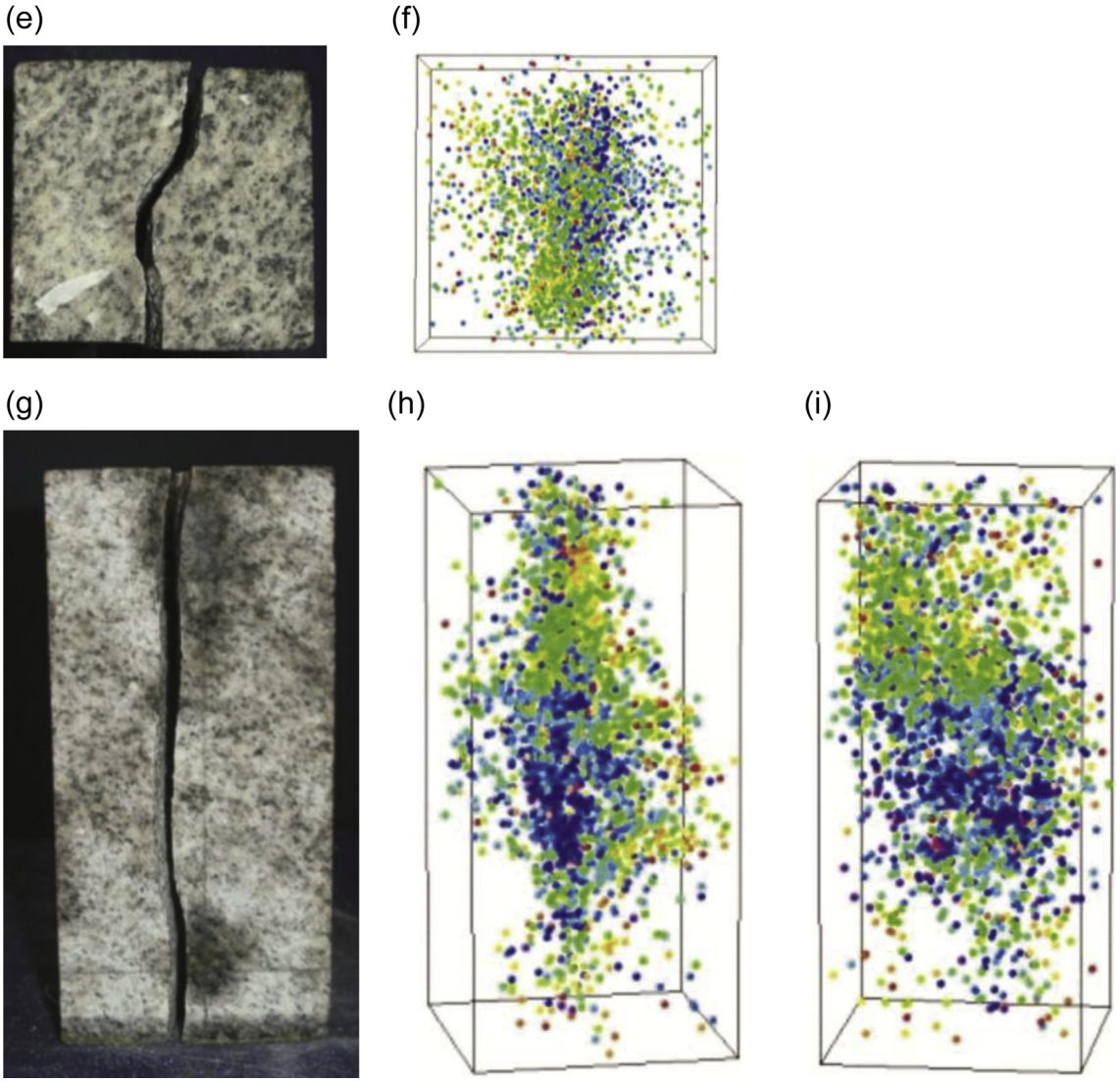


**Fig. 1 – (*continued*).**

technology in the real-time monitoring and early warning, the research on the acoustic emission characteristics during the rock failure progressive process will help to reveal the correlation between the monitored main acoustic emission parameters during the different failure stages, further understand the rock failure mechanism and put forward reasonable and effective damage precursor criteria. In this paper, the characteristics of the acoustic emission during the failure progressive process of rocks under uniaxial loading are firstly monitored. They are then analyzed through a series of the wavelet transforms to extract the acoustic emission frequency band energies during the different rock damage and failure stages. After that, the variation laws are derived for the changes of the frequency distribution and the frequency band energy ratio of the acoustic emission with the loading time, which provides a valuable basis for systematic exploration of the rock mass stability monitoring and early warning using the acoustic emission.

In the following, the uniaxial compression strength test of a granite is first conducted to generate real AE signals, which are then recorded using an AE monitoring system. After that, a new wavelet analysis method is developed and implemented into MATLAB for the frequency band and energy characteristics analysis of AE signals. Finally, the proposed wavelet analysis method is applied to analyze the AE signals recorded during the uniaxial loading of the granite extracting characteristic parameters, evaluating magnitude spectrum ratios, and determining energy ratios.

## 2. Wavelet analysis method for energy characteristics of AE signals

### 2.1. *AE signal monitoring experiments*

In order to obtain real AE signals for subsequent wavelet analyses, a granite is uniaxially loaded till failure in the laboratory and the released AE signals associated with the failure process of the granite are recorded using an AE monitoring system, as shown in Fig. 1. The granite is

taken from a quarry and has a uniaxial compressive strength of about 100 MPa, a tensile strength of about 10 MPa, and a P-wave velocity of about 3540 m/s. Rectangular samples with a size of 70 mm (length) × 70 mm (width) × 150 mm (height) were prepared and the opposing faces were ground parallel with errors within ±0.05 mm. Total six samples had been prepared from the granite. The rectangular granite samples were then uniaxially loaded in accordance with the suggested methods by International Society of Rock Mechanics (Bieniauski and Bernede, 1979). The AE signals released during the loading process were acquired in real time using a multi-channel, high-speed AE monitoring system, namely hyperion ultrasonic system (HUS) manufactured by ESG in Canada, as shown in Fig. 1. The HUS consists of AE sensors, preamplifiers, processing instrumentation, and AE software. Through the AE sensors, the AE signals were then converted into electrical signals. After that, the electrical signals were amplified by a preamplifier and converted into a digital data stream in an acoustic emission channel board (AECB). Finally, the AE features such as arrival times, rise times, duration, peak amplitude, energy and counts were extracted by a field programmable gate array (FPGA). Nano 30 sensors are adopted, whose frequency range is 125–750 kHz. The trigger threshold of the sensors is set to 100 mV, the preamplifier gain is set to 40 dB, the rear amplifier gain is 20 dB, and the sampling frequency is set to 10 MHz.

Fig. 2 presents the relationship between the accumulative AE events and the loading stress. Fig. 3 depicts a typical example of the AE signals collected in real time by the eight AE sensors of the AE monitoring system during the uniaxial loading of the granite. The collected AE signals will be analyzed using a wavelet analysis method developed later in this study, which will be introduced in detail in Section 3. The recorded AE signals can be further analyzed to determine the hypocenters of the AE events. However, before locating the AE events, the AE signals must be filtered to remove noise signals and gain accurate arrival time of the P-wave. The Geiger positional algorithm is then used to calculate the position and occurring time of the recorded AE events according to the difference of the AE sensors' coordinate and the P-wave arrival time since it is much more accurate compared with other algorithms.

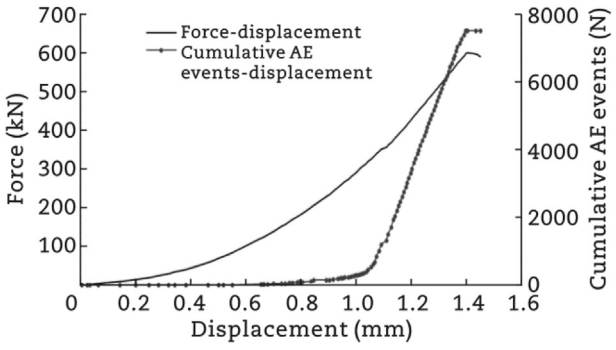


**Fig. 2 – Relationship between accumulative AE events and stress of integral rock samples.**

### 2.2. Discrete wavelet transform method

AE is attributed to the rapid release of the strain energy accumulated in the granite during loading. Thus, the energy content of the AE signal must be related to this energy release, too. The true energy of the AE signal is directly proportional to the area under the AE waveform (Miller and McIntire, 1987; Pollock, 1989). Correspondingly, the total energy of the AE signal can be obtained by integrating the square of the record AE signal (Duan and Zhu, 2000; Hu, 2006; Zhou et al., 2005), as shown in Eq. (1).

$$E = \int_{-\infty}^{\infty} x_0^2(t)\mathrm{d}t \tag{1}$$

where $x_0^2(t)$ is the recorded AE signal. According to the multi-resolution analysis, any AE signal can be decomposed using the discrete wavelet transform at the $J$ levels, and the $J+1$ frequency bands can be obtained. After the decomposition, the AE signal $x_0(t)$ can be expressed as the sum of detail signals at each level and large-scale approximate signals (Sang, 2012; Yang and Yu, 2012), as shown in Eq. (2).

$$x_0(t) = x_j^a(t) + \sum_{j=1}^{J} x_j^d(t) \tag{2}$$

where $x_j^a(t)$ is the reconstructed signal of the low frequency component after the discrete wavelet transform at the $j$ times, and $\sum_{j=1}^{J} x_j^d(t)$ is the reconstructed signal of the high frequency component after the discrete wavelet transform at the $J$ times.

Combining Eq. (1) with Eq. (2), Eq. (3) is obtained as follow.

$$E = \int_{-\infty}^{\infty} \left[x_j^a(t) + \sum_{j=1}^{J} x_j^d(t)\right]^2 \mathrm{d}t = \int_{-\infty}^{\infty} \left[x_j^a(t)\right]^2 \mathrm{d}t + \int_{-\infty}^{\infty} \left[\sum_{j=1}^{J} x_j^d(t)\right]^2 \mathrm{d}t + 2\sum_{j=1}^{J} \int_{-\infty}^{\infty} \left[x_j^d(t) x_j^a(t)\right] \mathrm{d}t + 2\sum_{j=j'} x_j^d(t) x_{j'}^d(t)\mathrm{d}t \tag{3}$$

According to the orthogonality properties of the wavelet and scaling functions, the latter two items of Eq. (3) should be equal to zero (Cui, 1995; Hu et al., 1999). Hence, Eq. (3) can be rewritten as Eq. (4) in the following.

$$E = \int_{-\infty}^{\infty} \left[x_j^a(t)\right]^2 \mathrm{d}t + \sum_{j=1}^{J} \int_{-\infty}^{\infty} \left[x_j^d(t)\right]^2 \mathrm{d}t = E_j^a + \sum_{j=1}^{J} E_j^d \tag{4}$$

Eq. (4) states that the energy of the AE signal is equal to the sum of the energy of the detail signals at each level and the energy of approximate signals at the large-scale. In practice, since the recorded AE signals are temporal series at discrete times, the energy of the detailed signals at the large-scale can be written as Eq. (5).

$$E_j^d = \Delta t \sum_k \left[x_j^d(k)\right]^2 \tag{5}$$

where $\Delta t$ is the sample interval of the AE signal. Similarly, the energy of the approximate signal at each level can be written as Eq. (6).

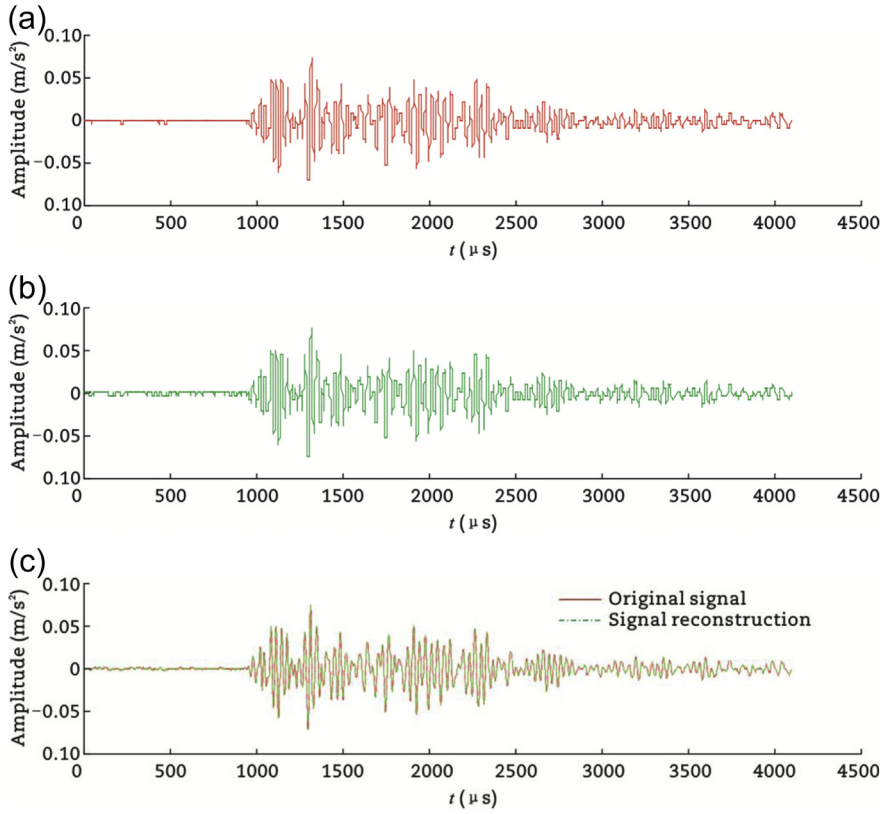


**Fig. 3 – Wavelet transform of a typical AE signal (i.e., AE event No. 1332) recorded during uniaxial loading of granite. (a) Original AE signal. (b) AE signal reconstruction. (c) Comparison of original and reconstructed signals.**

$$E_j^a = \Delta t \sum_k \left[x_j^a(k)\right]^2 \tag{6}$$

At each frequency band, the AE energy can be calculated using Eq. (6). The calculated AE energies at the $J+1$ frequency bands form a vector $[E_1, E_2, \cdots, E_J]$, which can be used to analyze the energy characteristics of the AE signals more reasonably compared with that before the discrete wavelet transform. This is because that the induced damage may suppress or enhanced the AE energy at some frequency bands when the AE signal is input into a system as excitation. In other words, the AE energy at some frequency bands may be suppressed while that at others may be enhanced. Correspondingly, there is a big difference between the energies calculated before and after the occurrence of the damage, i.e., the damage increases the relative energy of the signal at some frequency bands while it decreases the relative energy of the signal at other frequency bands. Thus, the energy of the signal at the decomposed frequency bands includes rich information of material damage and the change of the energy at a certain frequency band or a few frequency bands reflects the damage status of the material.

Moreover, according to (Wu et al., 2008), the ratio of the waveform energy at each frequency band $E_j^a$ to the original waveform energy $E$ can be defined as the energy spectrum coefficients in Eq. (7).

$$T' = [E_1/E, E_2/E, \cdots, E_J/E] \tag{7}$$

Eq. (7) represents the distribution of the signal's energy at different frequency bands. Different information which a signal contains will lead to different distribution of the signal's energy at different frequency bands. As for the AE signals, the different information of the AE signals reveal the different AE sources. Thus, the energy spectrum coefficients can be used to identify the different AE sources.

## 3. New application of the discrete wavelet transform method in analyzing energy characteristics of AE signals

As introduced above, a number of AE signals are recorded during the uniaxial loading of the granite using the real-time AE monitoring system. The recorded AE signals are then analyzed using the discrete wavelet transform developed in-house in Section 2.2. The Meyer wavelet is chosen as the wavelet basis for the discrete wavelet transform due to its fast convergence on frequency domain, regularity, localization in time domain, and the most importantly infinite differentiation. The frequency range of the Meyer mother wavelet is [1/3, 4/3] Hz. Thus, for a sampling interval, $\Delta t$, the frequency range which the wavelet transform can denote is $[1/3, 4/3]/(a\Delta t)$ at any scale $a$, and the frequency bands at adjacent scales may overlap with each other. Because the energy of the Meyer wavelet is mainly concentrated in the centre of the frequency bands, and attenuated quickly from the centre of the frequency

**Table 1 – Frequency band number nomenclature and energy distribution in different scales.**

| Scale | Frequency range (kHz) | Frequency band No. | Energy ($m^2/s^4$) | Percentage (%) |
|---|---|---|---|---|
| a7 | 0–3.90625 | b1 | 0.002827 | 0.3266 |
| d7 | 3.90625–7.81250 | b2 | 0.004519 | 0.5221 |
| d6 | 7.81250–15.62500 | b3 | 0.071373 | 8.2456 |
| d5 | 15.62500–31.25000 | b4 | 0.542901 | 62.7199 |
| d4 | 31.25000–62.50000 | b5 | 0.243056 | 28.0796 |
| d3 | 62.50000–125.00000 | b6 | 0.000610 | 0.0705 |
| d2 | 125.00000–250.00000 | b7 | 0.000243 | 0.0281 |
| d1 | 250.00000–500.00000 | b8 | 0.000066 | 0.0077 |
| Σ | | | 0.865597 | 100.0010 |
| Original signal | | | 0.866200 | |

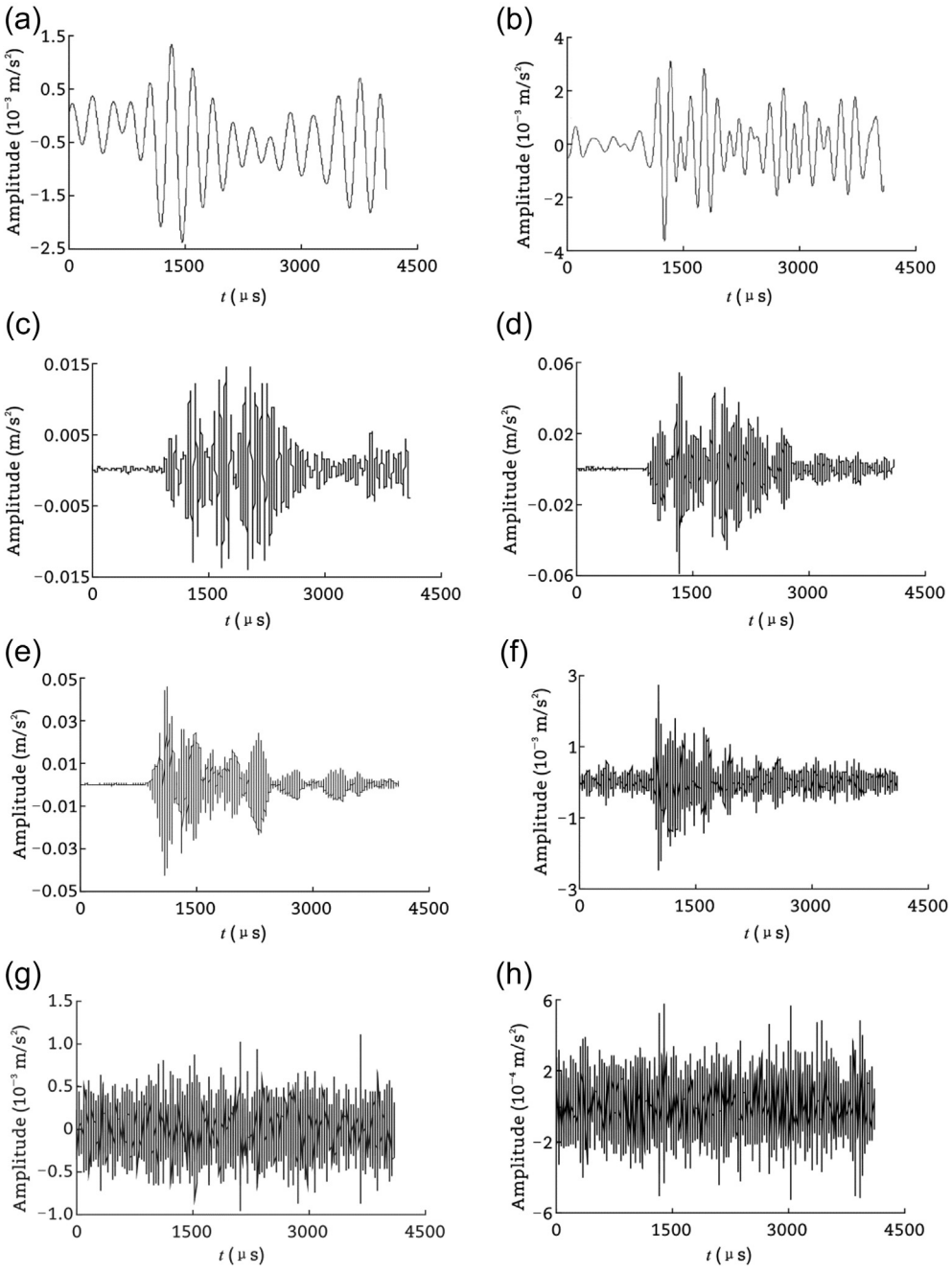


**Fig. 4 – Decomposition of the typical AE signal (Fig. 3 (a)) at seven scales using the proposed wavelet transform. (a) Approximate signal (a7). (b) Detailed signal (d7). (c) Detailed signal (d6). (d) Detailed signal (d5). (e) Detailed signal (d4). (f) Detailed signal (d3). (g) Detailed signal (d2). (h) Detailed signal (d1).**

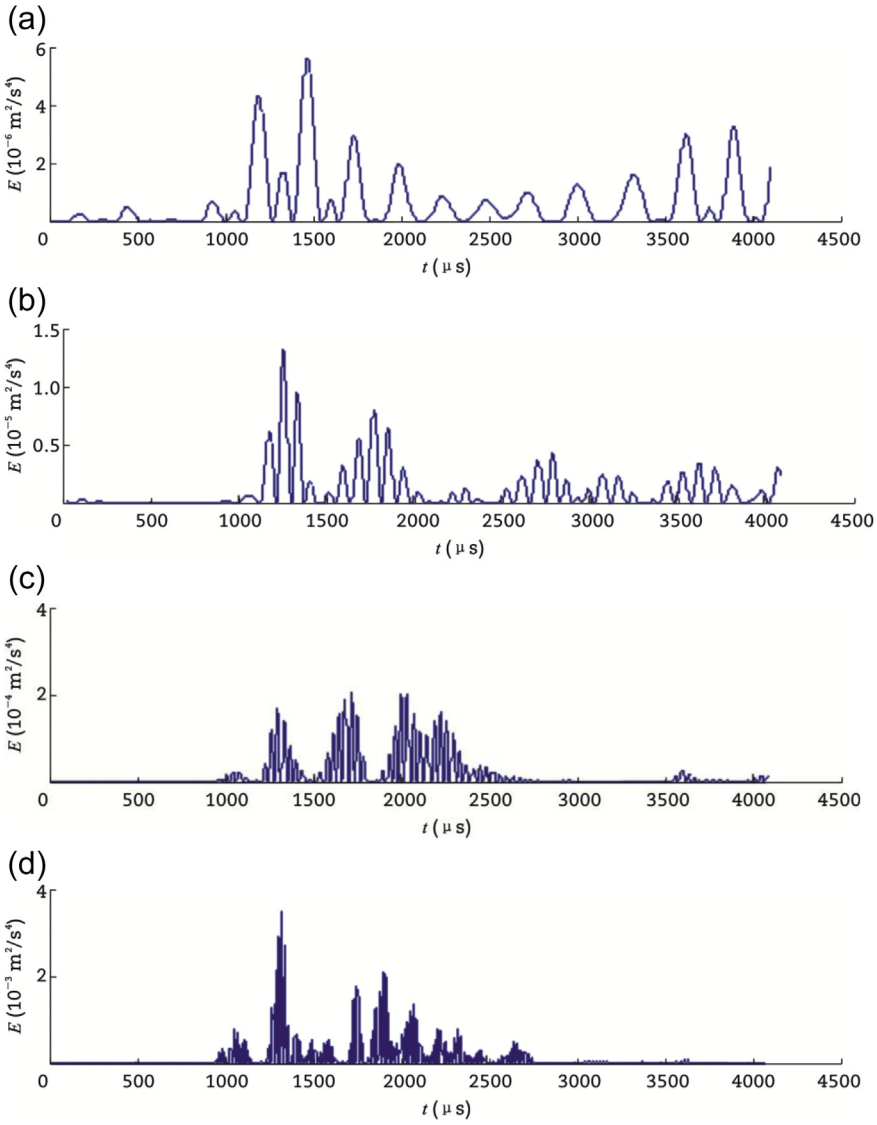


**Fig. 5 – Distribution of the AE energy in the time domain at each of the seven scales after the wavelet transform. (a) Approximate signal (a7). (b) Detailed signal (d7). (c) Detailed signal (d6). (d) Detailed signal (d5). (e) Detailed signal (d4). (f) Detailed signal (d3). (g) Detailed signal (d2). (h) Detailed signal (d1).**

band to the two boundaries. Correspondingly, the overlap of frequency bands at adjacent scale has little influence on the calculated energy since the overlap area is small and the mis-calculated energy is small, too. Thus, the intersection point of the frequency bands at the adjacent scales is taken as the boundary of the frequency bands of the Meyer wavelet. Table 1 summarizes the frequency ranges of each frequency band at each scale.

In the following, a typical AE signal, i.e., the AE event No. 1332, recorded during the uniaxial loading of the granite will be decomposed at 7 scales using the new wavelet transform method developed in Section 2.2, i.e., the scale of the signal is discretised using 2, $a = 2^j$ and the obtained actual frequency ranges corresponding to each scale are summarized into Table 1. The AE signal before the wavelet analysis is depicted in Fig. 3(a). During the analysis, the AE waveforms are firstly loaded into MATLAB workspace. MATLAB is selected since it not only provides a quite versatile wavelet toolbox with numerous options but also offers the opportunity of programming and creating routines and codes for any application. After all AE waveforms are loaded in MATLAB, the discrete wavelet transform (DWT) is then applied for each signal, which decomposes the original AE signal into wavelets at various levels. Each level represents a certain frequency band and the sum of the wavelets at all levels reconstructs the original AE signal, as shown in Fig. 3(b). The decomposition process is in fact a repetitive procedure of filtering the AE signal with specially designed band-pass filters. The advantages of the discrete wavelet transform are that the inversion of the transform is quite accurate and full reconstruction of the original signal is feasible, as shown in Fig. 3(c).

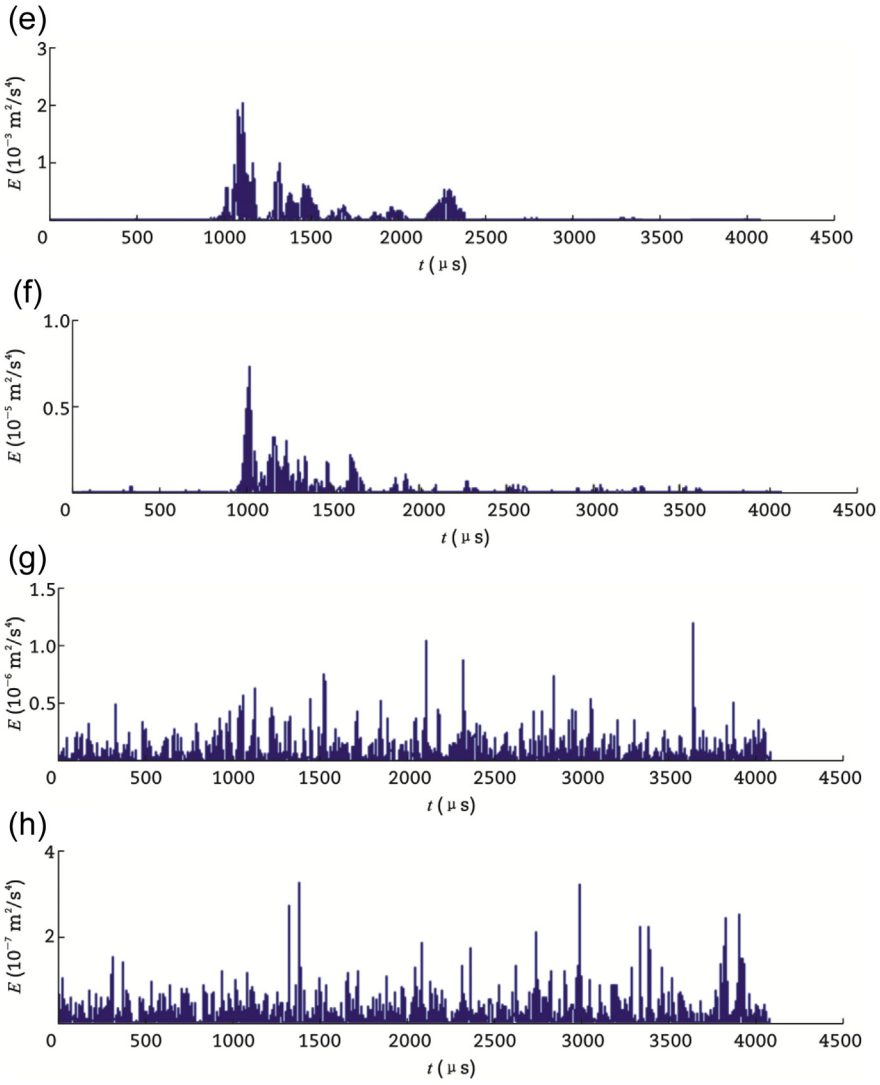


**Fig. 5 – *(continued)*.**

Fig. 4 depicts the Meyer wavelet decomposition of the original AE signal at seven levels. A discussion at this point may rise concerning the optimum wavelet to be used for a certain application and the optimum number of the decomposition levels since they are user-defined parameters in the proposed wavelet analysis method. As a matter fact, the proper wavelet type to be used has not been answered so far in a quantitative and explicit manner and no rules have been set to determine the superiority of one wavelet over another. One must comprehend quite well the properties and characteristics of the different wavelets, and have a profound knowledge of their differences and experiences to deal with a certain type of signals. As for the optimum number of levels, there are certain mathematical criteria called entropy criteria that can be used to determine if a decomposition is sufficient or more levels are needed. For a single AE signal, it is easy to check and define the optimum number of levels. However, in the case of a large number of AE signals, the entropy criteria are not easy to be applied as it is not obligatory that all waveforms must be decomposed at the same number of levels. In this study, after systematic trials, the number of levels was set to seven as it was evident that less were insufficient and more were redundant. As far as the type of wavelet is concerned, the Meyer wavelet was a very good compromise between the smooth function without sharp edges and the convenience of creating numerically the db wavelets of higher order.

Figs. 5 and 6 depict the distributions of the AE energy in the time domain and the frequency domain, respectively, at each of the seven decomposition scales. It is obvious that the AE signals are filtered through the different frequency bands at the different decomposition scales. The approximation scale, i.e., a7, has the lowest frequency band while the frequency increases from d7 to d1, i.e., from the approximate scale to the detail scale. The AE energy of the decomposed wavelet at each frequency band is calculated and plotted in Fig. 7, where the x-axis represents the waveforms as received in time (so it is a measure of time) and the y-axis represents the percentage of the AE energy at the scale as compared with the total energy of the AE signal. It is evident from Fig. 7 that the greatest

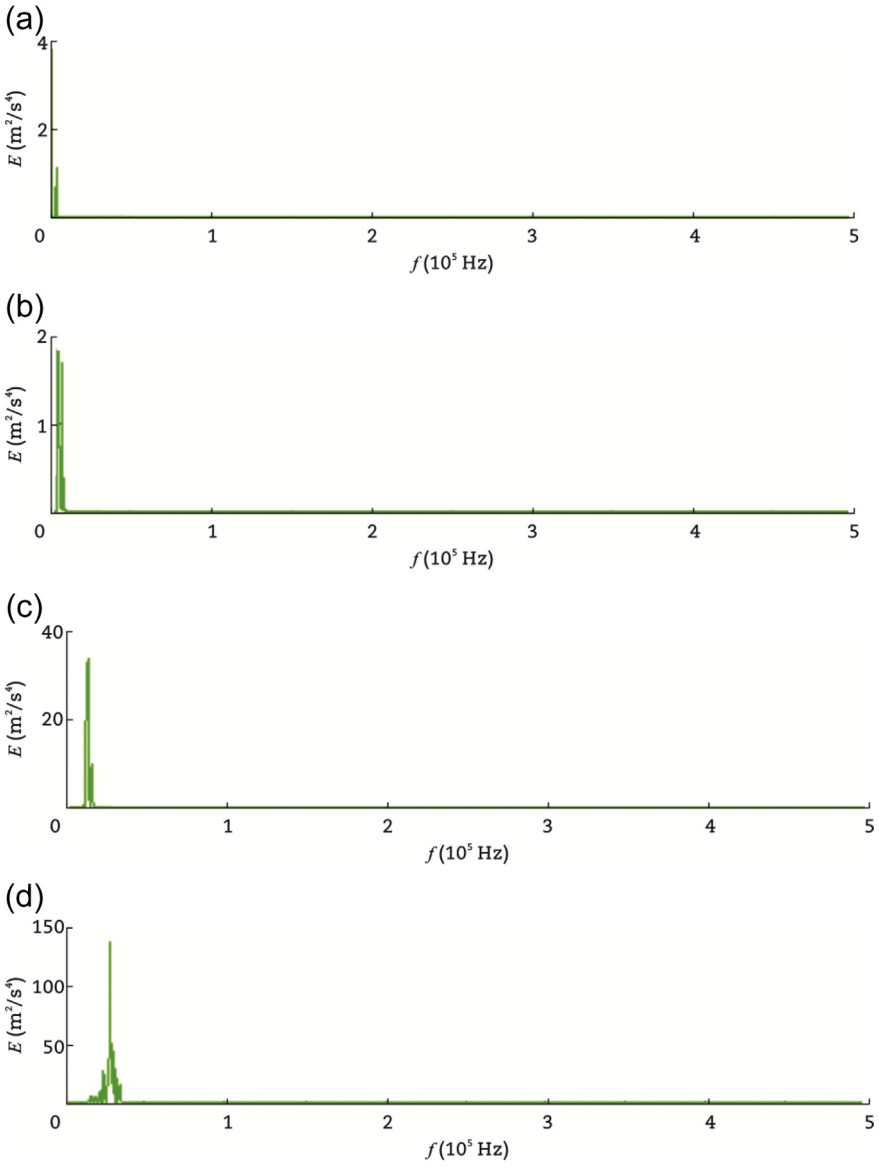


**Fig. 6 – Distribution of AE energy in the frequency domain at each of the seven scales after the wavelet transform. (a) Approximate signal (a7). (b) Detailed signal (d7). (c) Detailed signal (d6). (d) Detailed signal (d5). (e) Detailed signal (d4). (f) Detailed signal (d3). (g) Detailed signal (d2). (h) Detailed signal (d1).**

percentage of energy is gathered in three scales, namely detail d6 (b3), detail d5 (b4), and detail d4 (b5). These scales could be directly related to the damage mechanisms of the material as long as they carry more than 95% of the total signal energy and additionally they are characterized by different frequency bands. Then, the frequencies between 0 and 500 kHz are divided into eight equally spaced band and the AE energy in each band and its ratio in the total AE energy are calculated, which is listed in Table 1. It was found that, for the recorded AE signal, most energy lies in frequencies less than 62.5 kHz while almost no energy lies above 125 kHz. For the AE signals analyzed, energies are mainly distributed between the bands 7.8125–15.625 kHz (b3), 15.625–31.25 kHz (b4) and 31.25–62.5 kHz (b5). The b4 frequency band are the dominant one in the three frequency bands. Though, at this stage, it is not feasible to directly relate the energy levels to the damage mechanisms, it is believed that the energy content information obtained by the wavelet analysis is crucial for the identification of failure modes of the materials.

Moreover, it is found that the energy released due to the microcracking of the rock is mainly distributed in the frequency band in which the main rock fracture is located. For the granite tested in this study, the released energy from the microcracking was concentrated in the d5 frequency band. The percentage of the released energy is 62.72% of the total energy in the d5 frequency band. The percentage of the released energy is 28.08% and 8.24% of the total energy in the d4 and d6 frequency bands respectively. In the other frequency band, the percentage of the released energy is nearly zero. The main frequency band of the AE signals can be

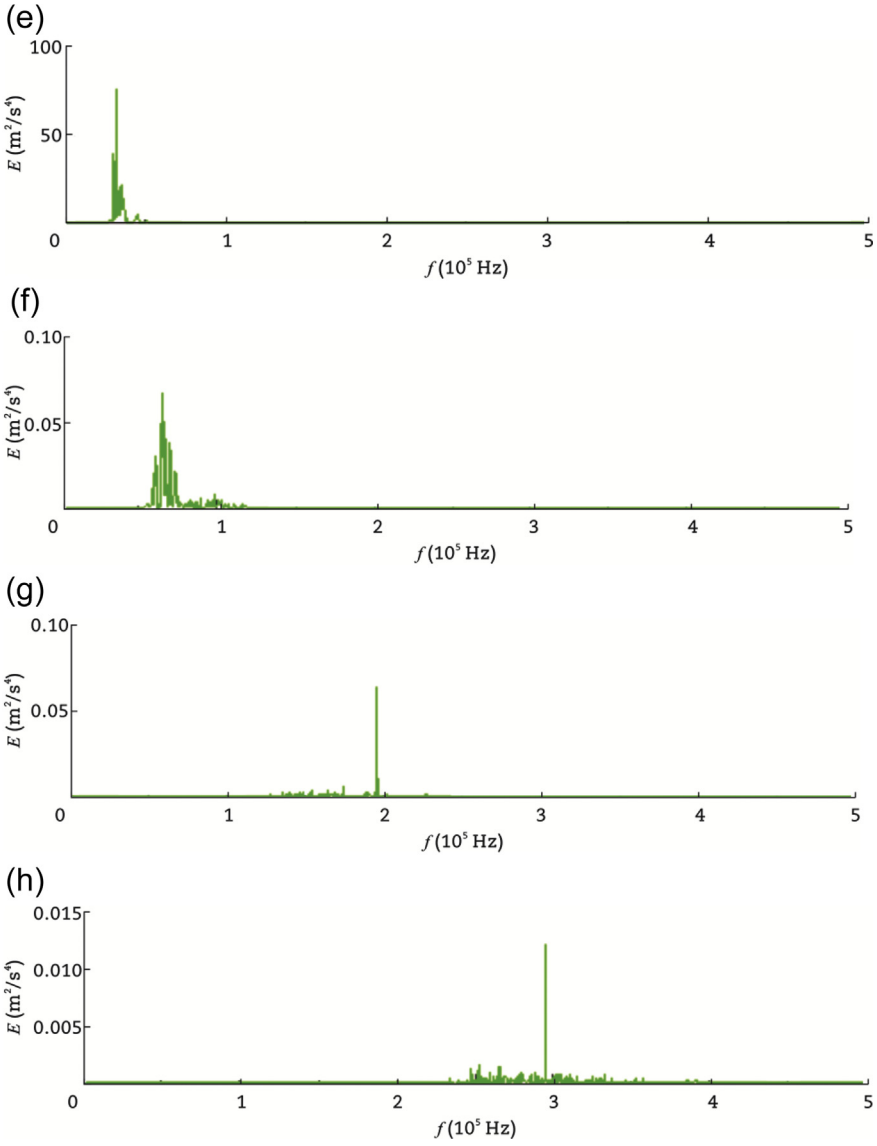


**Fig. 6 – *(continued)*.**

regarded as the characteristics of frequency band which can reflect the distribution characters of the AE energy.

Finally, it is noted that the sum of the AE energy in each frequency band after the wavelet transform is equal to the AE energy of the original AE signals. For the typical AE signal analyzed here, the sum of the AE energy at each frequency band decomposed using the proposed wavelet transform is 0.865597 $m^2/s^4$, which is 0.8662 $m^2/s^4$ for the original signal before the wavelet transform. Thus, the error is 0.0696%. As soon as enough experimental samples are obtained, the

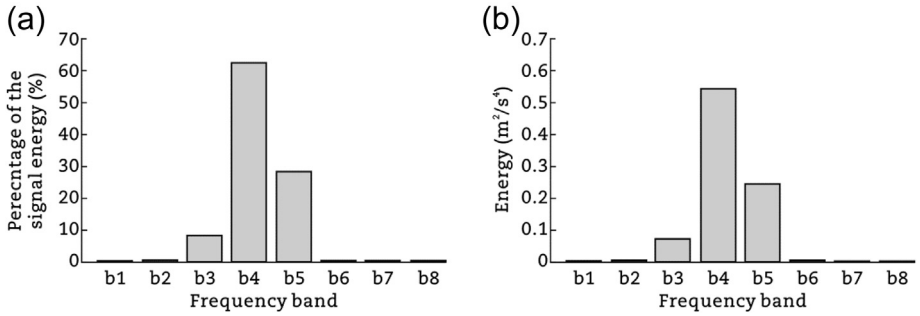


**Fig. 7 – Histograms of the AE energy at each frequency band. (a) Percentage of the AE energy. (b) Total AE energy.**

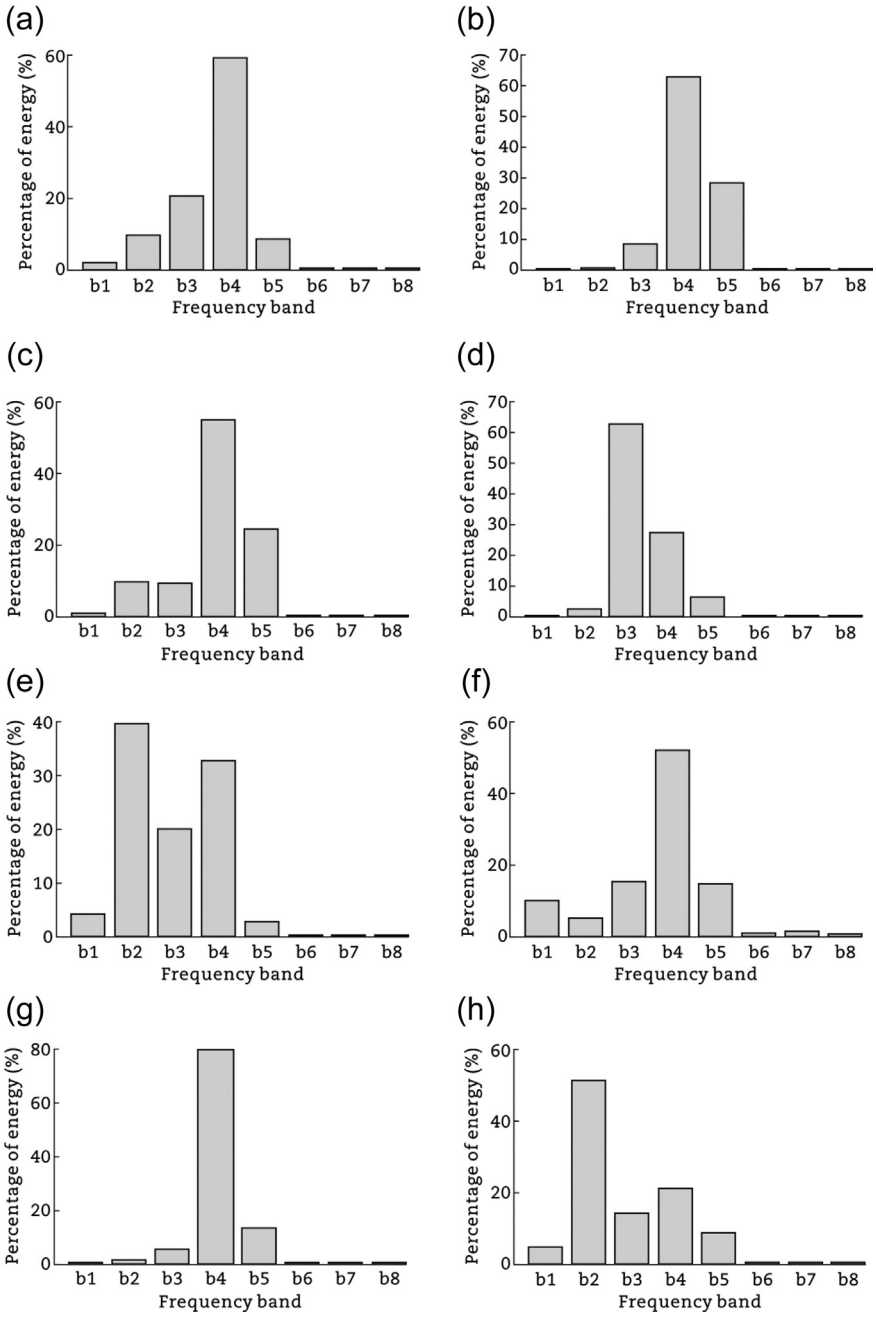


**Fig. 8 – Frequency band energy distribution of the acoustic emission signal at different damage stages. (a) Initial compression stage, event 1005. (b) Initial compression stage, event 1332. (c) Elastic deformation stage, event 2562. (d) Elastic deformation stage, event 2739. (e) Plastic deformation stage, event 4716. (f) Plastic deformation stage, event 5619. (g) Destruction stage, event 6070. (h) Destruction stage, event 6131.**

statistical characteristics of the energy distribution of the AE signals can be obtained for each type of rock, which can be used to guide the application of the AE technology in monitoring the stability of rock engineering structures in the field of geotechnical and mining engineering.

Similarly, the acoustic emission signals recorded during different loading stages are analyzed according to the methods presented above, and the frequency band energy distribution characteristics of the acoustic emission signals during different loading stages are obtained, as shown in Fig. 8. Fig. 9 shows the statistics of the variation trend of the dominant frequency band energy in the percentage during the loading test. It can be seen from Fig. 8 that the proportion of the energy in the dominant frequency band tends to increase with the load increasing. Similar to those conducted by the authors in a literature (Lai et al., 2014), the frequency band energy distribution of the acoustic emission signals and the variation law of the energy percentage of the

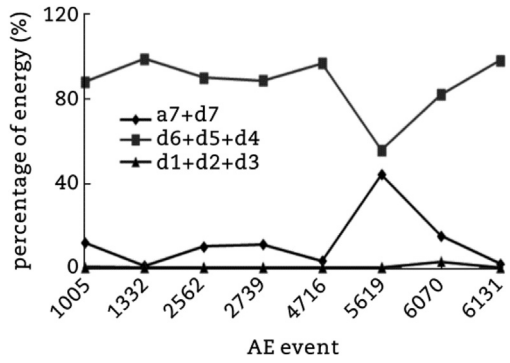


**Fig. 9 – Trends of the different frequency band energy percentage versus AE events at different damage stages.**

dominant frequency band during different loading stages can be summarized as the followings.

(1) The acoustic emission energy at each failure stage is concentrated in the frequency bands d4-d6, while the energy at other frequency bands is extremely few and decays rapidly with the diffusion of the crack.
(2) In the initial compaction stage (Fig. 8(a) and (b)), the energy at the d4-d6 decomposition scale, i.e., b3-b5 frequency bands is higher than that at the elastic deformation stage. The reason is that due to the pre-existing micropores and defects, the rock is gradually compacted under the action of external force, which makes the internal microstructure change and produce the lower frequency acoustic emission signals. At the elastic deformation stage, the internal grain dislocation and micro-cracks gradually increase, which is why the higher frequency acoustic emission signal dominates (Fig. 8(c) and (d)).

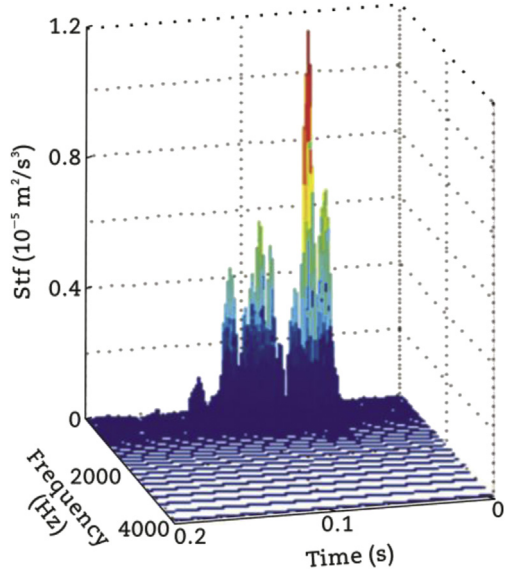


**Fig. 10 – Time-frequency energy distribution of AE signals on wavelet transform of Sensor 1.**

(3) At the plastic deformation stage, the macroscopic crack increases rapidly due to the continuous crack propagation, which creates new surfaces in the material, and is accompanied by high amplitude, long wavelength and low frequency elastic vibrations. In view of this, low-frequency acoustic emission signal is produced with the load increasing and the gradually increasing crack propagation results in the migration of the acoustic emissions to those at the lower frequency. As shown in Fig. 8(e), (h), the energy at the d4-d6 decomposition scale, i.e., b3-b5 frequency bands dominates till the coalescence of the macroscopic cracks resulting in the rock failure, which reveals that the failure mechanism is dominated by the microscopical crack propagation while new microcracks are seldom initiated.
(4) The energy proportion of the low frequency band increases but that of the dominant frequency band reduces. When the energy proportion of the dominant frequency band reaches a certain threshold (i.e., 50% or more), a critical point is reached between the internal crack propagation and the failure of rock. Moreover, according to the existing experimental results, a comprehensive analysis of the parameters, such as the acoustic emission counting rate and the acoustic emission event energy, shows that when the energy proportion of the dominant frequency band reaches 50% (or more), the main rupture has occurred and the larger macroscopic cracks have appeared inside the specimen. For different types of rocks, the threshold of the low frequency band energy ratio marking the main rupture should be different, which can be obtained by statistical analysis based on the tests of a large number of samples.
(5) The rock samples used in this experiment is intact granite. If the loading condition changes, no significant difference is found for the dominant frequency of the acoustic emission signals. Under the same loading conditions, the dominant frequency of the acoustic emission signals for different rocks increases with the increase of the rock strength. Therefore, although the characteristics of the acoustic emission frequency band and the corresponding energy summarized in this study are universal, the rock strength and actual loading conditions still need to be taken into account to determine the frequency band division and the critical point of the low frequency energy ratio in the specific application.

Besides, the time and frequency energy distribution of the acoustic emission signals is analyzed using the time-varying power spectrum method proposed in a literature (Kang et al., 2010). Fig. 10 illustrates the time-frequency energy distribution of a typical acoustic emission signal and Fig. 11 shows a contour plot of the time-varying power spectrum estimation of the acoustic emission signal with logarithmic coordinates on the vertical axis. This reflects the time-frequency energy distribution characteristics of the acoustic emission signals from another perspective. Based on the relationship between energy and time-frequency, the

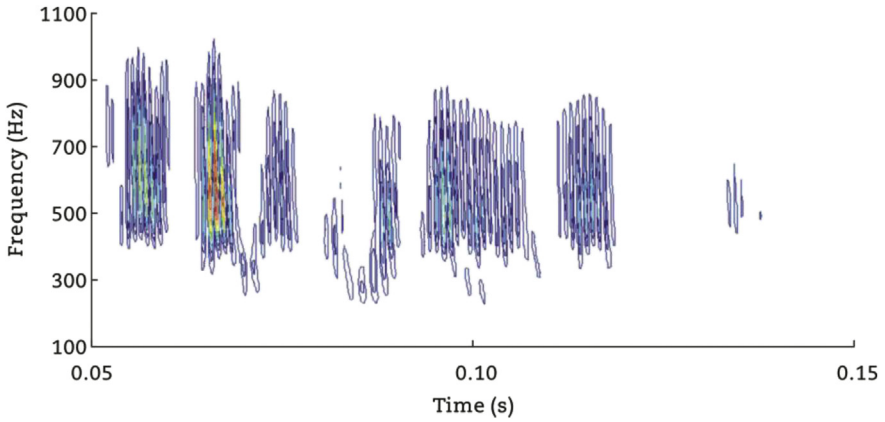


**Fig. 11 – Contour map of the wavelet transform of acoustic signal emitted from Sensor 1 (event 1332).**

relationship between the damage energy of rock burst and the band energy characteristics of acoustic emission signals can be further explored.

## 4. Conclusions

In this study, real AE signals are firstly generated by the uniaxial compression test of a granite specimen and monitored using an AE monitoring system. After that, a new wavelet scheme is developed on the basis of the discrete wavelet transform and implemented into MATLAB to analyzed the AE signals recorded during the uniaxial compression test of the granite. During the analysis, the recorded AE signals are decomposed into wavelets at seven levels. Each level represents a certain frequency band and the sum of the wavelets at all seven levels can accurately reconstructs the original AE signal without any signal loss. The approximate level, i.e., a7, has the lowest frequency band while the frequency increases up to 500 kHz from the approximate level to the detail level, i.e., from d7 to d1. After the decomposition process, the AE energy of the decomposed wavelet at each frequency band is calculated. It is found that the majority of the AE energy follows into three detail levels, i.e., b3 (d6), b4 (d5) and b5 (d4), which reveals that the AE energies at these levels are directly related to the damage mechanisms of the granite although further studies are need to identify the failure modes.

Finally, it is concluded that the proposed wavelet transform scheme provides a new method of analyzing frequency band and energy characteristics of the AE signals. Compared with the commonly used statistical distribution method of frequency spectrum based on the Fourier transform, the proposed wavelet transform method has obvious advantages in the time and frequency domains. The energy characteristics of the AE signals are mapped into various frequency bands using the proposed wavelet transform method, which makes the energy characteristics of un-obvious AE signals stand out under various resolutions, i.e. scales. Thus, the proposed wavelet transform method may provide a new means for the characteristics analysis of the microseismicity signals recorded by the microseismicity monitoring system and may stimulate the application of the AE technology in the geotechnical engineering through analyzing the energy of the AE signals to understand the law of AE emitted by the failure of rockmass.

The wavelet transform was used to analyze and process acoustic emission waveform signals monitored during uniaxial loading of granites to find out the frequency distribution characteristics of acoustic emission signals and the energy transition rule of the frequency bands in each destructive stage. The implemented wavelet transform can process the signals without oversight and redundancy and orthogonally decompose them into multiple independent components of the band, whose signal energy distribution and variation can accurately reflect the acoustic emission source. The rock destructive mechanism can be derived according to the relationship between the crack propagation and the frequency change of the acoustic emission signal. Lower frequency acoustic emission signals are generated by the expansion of larger macroscopic cracks. The total energy of the acoustic emission signals varies greatly during the different stages of destruction. By analyzing the energy proportion of the dominant frequency band and the variation of the energy proportion in different failure stages, a certain threshold of the low-frequency energy proportion is proposed as the precursor of the critical damage point, which is of great practical significance to the design of rock engineering instability monitoring and early warning system, and also provides a theoretical basis for assessing the internal damage of rock.

## Conflict of interest

The authors do not have any conflict of interest with other entities or researchers.

## Acknowledgments

The present work is partially supported by the National Natural Science Foundation of China (Grant Nos. 51204029, 51525402, 51374049, 51474050 and U1602232), the Science Career Public Welfare Research Foundation of Liaoning Province (No. 2015003001), and the Scientific Research Foundation

for the Returned Overseas Chinese Scholars, State Education Ministry (No. 50-2) which are gratefully appreciated. Moreover, the first author would like to thank the China Scholarship Council for supporting her academic visit to the University of Tasmania, where the analytical work is completed.

## REFERENCES

Amiri, G.G., Rad, A.A., Hazaveh, N.K., 2015. Wavelet-based method for generating nonstationary artificial pulse-like near-fault ground motions. Computer Aided Civil and Infrastructure Engineering 29 (10), 758–770.

Antonaci, P., Bocca, P., Masera, D., 2012. Fatigue crack propagation monitoring by acoustic emission signal analysis. Key Engineering Materials 81, 26–32.

Baddari, K., Frolov, A.D., Tourtchine, V., et al., 2011. An integrated study of the dynamics of electromagnetic and acoustic regimes during failure of complex macro systems using rock blocks. Rock Mechanics and Rock Engineering 44, 269–280.

Basu, S., Ali, M.Y., Farid, A., et al., 2014. A microseismic experiment in Abu Dhabi, United Arab Emirates: implications for carbonate reservior monitoring. Arabian Journal of Geosciences 7 (9), 3815–3827.

Bieniauski, Z.T., Bernede, M.J., 1979. Suggested method for determining the uniaxial compressive strength and deformability of rock materials. International Journal of Rock Mechanics and Mining Sciences & Geomechanics Abstracts 16 (2), 138–140.

Cai, M., Kaiser, P.K., Morioka, H., et al., 2007. FLAC/PFC coupled numerical simulation of AE in large-scale underground excavations. International Journal of Rock Mechanics and Mining Sciences 44 (4), 550–564.

Chorney, D.R., Grob, M., Jam, P., et al., 2014. Numerical analysis of acoustic emissions, the radiated energy and their moment tensors in triaxial deformation tests. In: 48th US Rock Mechanics/Geomechanics Symposium, Minnesota City, 2014.

Cui, J.T., 1995. An Introduction to Wavelet. Xi'an Jiaotong University Press, Xi'an.

Davi, R., Vavryčuk, V., Charalampidou, E.M., et al., 2013. Network sensor calibration for retrieving accurate moment tensors of acoustic emissions. International Journal of Rock Mechanics and Mining Sciences 62 (5), 59–67.

Ding, Y., Reuben, R.L., Steel, J.A., 2004. A new method for waveform analysis for estimating AE wave arrival times using wavelet decomposition. NDT & E International 37 (4), 279–290.

Duan, X.P., Zhu, H.P., 2000. Application of wavelets to structural dynamic analysis under seismic excitations. Journal of Huazhong University of Science and Technology 28 (11), 75–78.

Guo, J., Ding, L., Luo, H., et al., 2014. Wavelet prediction method for ground deformation induced by tunneling. Tunnelling and Underground Space Technology 41 (1), 137–151.

Hryciw, R.D., Ohm, H.S., Zhou, J., 2015. Theoretical basis for optical granulometry by wavelet transformation. Journal of Computing in Civil Engineering 29 (3), 04014050.

Hu, C.H., Zhang, J.B., Xia, J., 1999. System Analysis and Design Based on MATLAB-Wavelet Analysis. Xi'an University of Electronic Science and Technology Press, Xi'an.

Hu, Y.X., 2006. Earthquake Engineering, second ed. Earthquake Press, Beijing.

Jeong, H., Jang, Y.S., 2000. Wavelet analysis of plate wave propagation in composite laminates. Composite Structures 49, 443–450.

Kalenchuk, K.S., Crockford, A.M., Hume, C.D., et al., 2014. Application of numerical modelling to predicted seismic probability and mitigate associated risks during the Craig pillar extraction at Morrison Mine, KGHM International. In: 48th US Rock Mechanics/Geomechanics Symposium, Minnesota, 2014.

Kang, Y.M., Zhu, W.C., Bai, Q., et al., 2010. Time delay estimation of acoustic emission signals of rock using time-frequency analysis based on wavelet transform. Chinese Journal of Rock Mechanics and Engineering 29 (5), 1010–1016.

Karimi, N.Z., Minak, G., Kianfar, P., 2015. Analysis of damage mechanisms in drilling of composite materials by acoustic emission. Composite Structures 131, 107–114.

Kwiatek, G., Charalampidou, E.M., Dresen, G., et al., 2014. An improved method for seismic moment tensor inversion of acoustic emissions through assessment of sensor coupling and sensitivity to incidence angle. International Journal of Rock Mechanics and Mining Sciences 65 (1), 153–161.

Lai, Y.S., Xiong, Y., Cheng, L.F., 2014. Frequency band energy characteristics of acoustic emission signals in damage process of concrete under uniaxial compression. Journal of Vibration and Shock 32 (2), 12–19.

Lesniak, A., Isakow, Z., 2009. Space-time clustering of seismic events and hazard assessment in the Zabrze-Bielszowicecoal mine, Poland. International Journal of Rock Mechanics and Mining Sciences 46 (5), 918–928.

Lockner, D., 1993. The role of acoustic emission in the study of rock fracture. International Journal of Rock Mechanics and Mining Sciences 30 (7), 883–899.

Lynch, R.A., Wuite, R., Smith, B.S., et al., 2005. Micro-seismic monitoring of open pit slopes. In: The 6th Symposium on Rockbursts and Seismicity in Mines, Perth, 2005.

Miller, R.K., McIntire, P., 1987. Non-destructive Testing Handbook: Volume 5 Acoustic Emission Testing. American Society for Non-destructive Testing Inc., Columbus.

Ni, Q.Q., Iwamoto, M., 2002. Wavelet transform of acoustic emission signals in failure of model composites. Engineering Fracture Mechanics 69, 717–728.

Pollock, A.A., 1989. Acoustic Emission Inspection. TR-103-96-12/89. Physical Acoustics Corporation, Princeton.

Prawin, J., Rao, A.R.M., 2015. Time frequency analysis for nonlinear identification of structures. Journal of Structural Engineering 42 (1), 40–48.

Qi, G., Barhorst, A., Hashemi, J., et al., 1997. Discrete wavelet decomposition of acoustic emission signals from carbon-fiber-reinforced composites. Composites Science and Technology 57 (4), 389–403.

Rao, M.V.M.S., Murthy, D.S.N., Rao, G.M.N., et al., 2004. Stress-induced micro-cracking and brittle failure of godhra granite, Gujarat: a laboratory investigation using acoustic emission. Journal of the Geological Society of India 64 (6), 775–783.

Sang, Y.F., 2012. A practical guide to discrete wavelet decomposition of hydrologic time series. Water Resources Management 26 (11), 3345–3365.

Tang, C.A., Wang, J.M., Zhang, J.J., 2011. Preliminary engineering application of microseismic monitoring technique to rockburst prediction in tunnelling of Jinping II project. Journal of Rock Mechanics and Geotechnical Engineering 2 (3), 193–208.

Vafaei, M., Adnan, A.B., 2014. Seismic damage detection of tall airport traffic control towers using wavelet analysis. Structure and Infrastructure Engineering 10 (1), 106–127.

Wu, Z.W., Wang, S.M., Shen, G.T., 2008. Extraction of acoustic emission resource characteristics based on wavelet transform. Journal of Wuhan University of Technology (Transportation Science & Engineering Edition) 32 (1), 85–87.

Xu, N.W., Tang, C.A., Li, L.C., et al., 2011. Microseismic monitoring and stability analysis of the left bank slope in Jinping first

stage hydropower station in southwestern China. International Journal of Rock Mechanics and Mining Sciences 48 (6), 950–963.
Yang, Z., Yu, Z., 2012. Grinding wheel wear monitoring based on wavelet analysis and support vector machine. International Journal of Advanced Manufacturing Technology 62 (1–4), 107–121.
Zhou, R.Z., Wu, C., Zhou, X.P., 2005. Wavelet decomposition method for solution to structural dynamic response. Earthquake Engineering and Engineering Vibration 25 (6), 43–48.
Zou, L., Jing, L., Cvetkovic, V., 2015. Roughness decomposition and nonlinear fluid flow in a single rock fracture. International Journal of Rock Mechanics and Mining Sciences 75, 102–118.

Dr. Yumei Kang is currently an associate professor in the College of Resources and Civil Engineering at Northeastern University (NEU) in China. She completed his PhD, master and bachelor degrees at Northeastern University in China. She has published over 30 articles in Chinese and international journals, many of which were indexed by SCI/EI, and presided over more than 10 national, provincial and ministerial level projects. Her specialties include rock failure process analysis and structural damage identification.

Dr. Hongyuan Liu is currently a senior lecturer at University of Tasmania (UTAS) in Australia. He completed his PhD at Lulea University of Technology in Sweden and master and bachelor degrees at Northeastern University in China. Before jointed in UTAS as a lecturer, he had worked as a research fellow and postdoctoral fellow in University of Queensland and University of Sydney, respectively. He has published over 50 articles in international journals, which leads to an H-index of 20 and 822 citations in Scopus. He is currently supervising 3 PhD students and leads a geomechanics research group at UTAS.